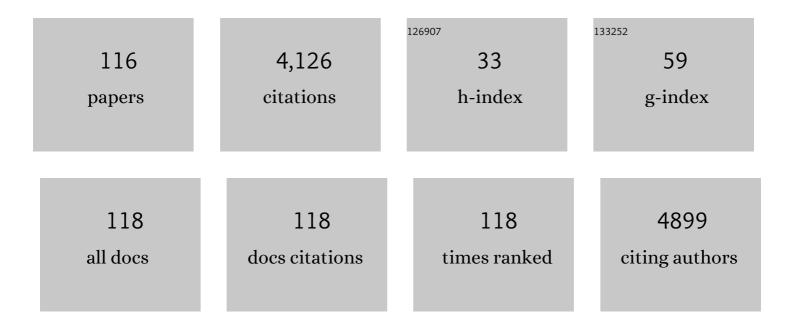
List of Publications by Year in descending order

Source: https://exaly.com/author-pdf/3455972/publications.pdf Version: 2024-02-01



LUN LANC

#	Article	IF	CITATIONS
1	Regulating Photocatalysis by Spin-State Manipulation of Cobalt in Covalent Organic Frameworks. Journal of the American Chemical Society, 2020, 142, 16723-16731.	13.7	333
2	Graphitic carbon nitride supported single-atom catalysts for efficient oxygen evolution reaction. Chemical Communications, 2016, 52, 13233-13236.	4.1	176
3	Realizing a Not-Strong-Not-Weak Polarization Electric Field in Single-Atom Catalysts Sandwiched by Boron Nitride and Graphene Sheets for Efficient Nitrogen Fixation. Journal of the American Chemical Society, 2020, 142, 19308-19315.	13.7	170
4	Gate-controlled VO ₂ phase transition for high-performance smart windows. Science Advances, 2019, 5, eaav6815.	10.3	160
5	Electronic Spin Moment As a Catalytic Descriptor for Fe Single-Atom Catalysts Supported on C ₂ N. Journal of the American Chemical Society, 2021, 143, 4405-4413.	13.7	138
6	Charged Metalloporphyrin Polymers for Cooperative Synthesis of Cyclic Carbonates from CO ₂ under Ambient Conditions. ChemSusChem, 2017, 10, 2534-2541.	6.8	122
7	Cooperative Spin Transition of Monodispersed FeN ₃ Sites within Graphene Induced by CO Adsorption. Journal of the American Chemical Society, 2018, 140, 15149-15152.	13.7	108
8	Graphene–boron nitride hybrid-supported single Mo atom electrocatalysts for efficient nitrogen reduction reaction. Journal of Materials Chemistry A, 2019, 7, 15173-15180.	10.3	107
9	Function-oriented ionic polymers having high-density active sites for sustainable carbon dioxide conversion. Journal of Materials Chemistry A, 2018, 6, 9172-9182.	10.3	91
10	New bi-functional zinc catalysts based on robust and easy-to-handle N-chelating ligands for the synthesis of cyclic carbonates from epoxides and CO ₂ under mild conditions. Green Chemistry, 2014, 16, 4179-4189.	9.0	88
11	Synergistic Effect of Surface-Terminated Oxygen Vacancy and Single-Atom Catalysts on Defective MXenes for Efficient Nitrogen Fixation. Journal of Physical Chemistry Letters, 2020, 11, 5051-5058.	4.6	88
12	Two-Dimensional All-in-One Sulfide Monolayers Driving Photocatalytic Overall Water Splitting. Nano Letters, 2021, 21, 6228-6236.	9.1	88
13	Non-catalytic hydrogenation of VO2 in acid solution. Nature Communications, 2018, 9, 818.	12.8	87
14	Combining photocatalytic hydrogen generation and capsule storage in graphene based sandwich structures. Nature Communications, 2017, 8, 16049.	12.8	86
15	Organic field-effect optical waveguides. Nature Communications, 2018, 9, 4790.	12.8	85
16	Carbon nanotube-encapsulated cobalt for oxygen reduction: integration of space confinement and N-doping. Chemical Communications, 2019, 55, 14801-14804.	4.1	85
17	Photocatalytic Properties and Mechanistic Insights into Visible Lightâ€Promoted Aerobic Oxidation of Sulfides to Sulfoxides via Tin Porphyrinâ€Based Porous Aromatic Frameworks. Advanced Synthesis and Catalysis, 2018, 360, 4402-4411.	4.3	67
18	Metal-Free Boron Nitride Nanoribbon Catalysts for Electrochemical CO ₂ Reduction: Combining High Activity and Selectivity. ACS Applied Materials & Interfaces, 2019, 11, 906-915.	8.0	66

#	Article	IF	CITATIONS
19	Tunable Hydrogen Doping of Metal Oxide Semiconductors with Acid–Metal Treatment at Ambient Conditions. Journal of the American Chemical Society, 2020, 142, 4136-4140.	13.7	65
20	Electric Dipole Descriptor for Machine Learning Prediction of Catalyst Surface–Molecular Adsorbate Interactions. Journal of the American Chemical Society, 2020, 142, 7737-7743.	13.7	65
21	Regulating Electronic Spin Moments of Single-Atom Catalyst Sites via Single-Atom Promoter Tuning on S-Vacancy MoS ₂ for Efficient Nitrogen Fixation. Journal of Physical Chemistry Letters, 2021, 12, 8355-8362.	4.6	63
22	Machine Learning Protocol for Surface-Enhanced Raman Spectroscopy. Journal of Physical Chemistry Letters, 2019, 10, 6026-6031.	4.6	60
23	A neural network protocol for electronic excitations of <i>N</i> -methylacetamide. Proceedings of the United States of America, 2019, 116, 11612-11617.	7.1	55
24	A Machine Learning Protocol for Predicting Protein Infrared Spectra. Journal of the American Chemical Society, 2020, 142, 19071-19077.	13.7	55
25	Impact of Active Site Density on Oxygen Reduction Reactions Using Monodispersed Fe–N–C Single-Atom Catalysts. ACS Applied Materials & Interfaces, 2020, 12, 15271-15278.	8.0	55
26	Cobalt–Salen-Based Porous Ionic Polymer: The Role of Valence on Cooperative Conversion of CO ₂ to Cyclic Carbonate. ACS Applied Materials & Interfaces, 2020, 12, 609-618.	8.0	53
27	Boosted Reactivity of Ammonia Borane Dehydrogenation over Ni/Ni ₂ P Heterostructure. Journal of Physical Chemistry Letters, 2019, 10, 1048-1054.	4.6	52
28	Highly Active Graphene Oxide-Supported Cobalt Single-Ion Catalyst for Chemiluminescence Reaction. Analytical Chemistry, 2017, 89, 13518-13523.	6.5	51
29	Efficient and Accurate Simulations of Vibrational and Electronic Spectra with Symmetry-Preserving Neural Network Models for Tensorial Properties. Journal of Physical Chemistry B, 2020, 124, 7284-7290.	2.6	51
30	Single nickel atom supported on hybridized graphene–boron nitride nanosheet as a highly active bi-functional electrocatalyst for hydrogen and oxygen evolution reactions. Journal of Materials Chemistry A, 2019, 7, 26261-26265.	10.3	44
31	C ₂ N-supported single metal ion catalysts for HCOOH dehydrogenation. Journal of Materials Chemistry A, 2018, 6, 11105-11112.	10.3	40
32	Highly Selective and Efficient Synthesis of 7-Aminoquinolines and Their Applications as Golgi-Localized Probes. ACS Medicinal Chemistry Letters, 2019, 10, 954-959.	2.8	40
33	Toward Rational Design of Dual-Metal-Site Catalysts: Catalytic Descriptor Exploration. ACS Catalysis, 2022, 12, 3420-3429.	11.2	40
34	Enhanced Activity of C ₂ N-Supported Single Co Atom Catalyst by Single Atom Promoter. Journal of Physical Chemistry Letters, 2019, 10, 7009-7014.	4.6	35
35	A boron-centered radical: a potassium-crown ether stabilized boryl radical anion. Chemical Communications, 2016, 52, 12714-12716.	4.1	34
36	Material descriptors for photocatalyst/catalyst design. Wiley Interdisciplinary Reviews: Computational Molecular Science, 2018, 8, e1369.	14.6	34

#	Article	IF	CITATIONS
37	Porous Metallosalen Hypercrosslinked Ionic Polymers for Cooperative CO ₂ Cycloaddition Conversion. Industrial & Engineering Chemistry Research, 2020, 59, 676-684.	3.7	34
38	Dual-Atom Metal and Nonmetal Site Catalyst on a Single Nickel Atom Supported on a Hybridized BCN Nanosheet for Electrochemical CO ₂ Reduction to Methane: Combining High Activity and Selectivity. ACS Applied Materials & Interfaces, 2022, 14, 9073-9083.	8.0	34
39	Protecting Single Atom Catalysts with Graphene/Carbon-Nitride "Chainmailâ€: Journal of Physical Chemistry Letters, 2019, 10, 3129-3133.	4.6	33
40	Exceeding the volcano relationship in oxygen reduction/evolution reactions using single-atom-based catalysts with dual-active-sites. Journal of Materials Chemistry A, 2020, 8, 10193-10198.	10.3	33
41	Isolating hydrogen from oxygen in photocatalytic water splitting with a carbon-quantum-dot/carbon-nitride hybrid. Journal of Materials Chemistry A, 2019, 7, 6143-6148.	10.3	32
42	Aggregation-Induced Enhancement of Molecular Phosphorescence Lifetime: A First-Principle Study. Journal of Physical Chemistry C, 2018, 122, 25796-25803.	3.1	29
43	Aggregation-Induced Intersystem Crossing: Rational Design for Phosphorescence Manipulation. Journal of Physical Chemistry B, 2020, 124, 2238-2244.	2.6	29
44	Catalytic Chemistry Predicted by a Charge Polarization Descriptor: Synergistic O ₂ Activation and CO Oxidation by Au–Cu Bimetallic Clusters on TiO ₂ (101). ACS Applied Materials & Interfaces, 2019, 11, 9629-9640.	8.0	28
45	Direct aerobic liquid phase epoxidation of propylene catalyzed by Mn(<scp>iii</scp>) porphyrin under mild conditions: evidence for the existence of both peroxide and Mn(<scp>iv</scp>)-oxo species from in situ characterizations. RSC Advances, 2015, 5, 30014-30020.	3.6	27
46	Combining High Photocatalytic Activity and Stability via Subsurface Defects in TiO ₂ . Journal of Physical Chemistry C, 2018, 122, 17221-17227.	3.1	27
47	Electron–Proton Coâ€dopingâ€Induced Metal–Insulator Transition in VO ₂ Film via Surface Selfâ€Assembled <scp>I</scp> â€Ascorbic Acid Molecules. Angewandte Chemie - International Edition, 2019, 58, 13711-13716.	13.8	27
48	Cooperative Single-Atom Active Centers for Attenuating the Linear Scaling Effect in the Nitrogen Reduction Reaction. Journal of Physical Chemistry Letters, 2021, 12, 5233-5240.	4.6	25
49	Insight into Electronic and Structural Reorganizations for Defect-Induced VO ₂ Metal–Insulator Transition. Journal of Physical Chemistry Letters, 2017, 8, 3129-3132.	4.6	24
50	Graphene Oxide-Supported Transition Metal Catalysts for Di-Nitrogen Reduction. Journal of Physical Chemistry C, 2018, 122, 25441-25446.	3.1	24
51	A Carbazolyl Porphyrinâ€Based Conjugated Microporous Polymer for Metalâ€Free Photocatalytic Aerobic Oxidation Reactions. ChemCatChem, 2020, 12, 3523-3529.	3.7	24
52	Metalloporphyrin-mediated aerobic oxidation of hydrocarbons in cumene: Co-substrate specificity and mechanistic consideration. Molecular Catalysis, 2017, 440, 36-42.	2.0	23
53	Sulfur Atomically Doped Bismuth Nanobelt Driven by Electrochemical Self-Reconstruction for Boosted Electrocatalysis. Journal of Physical Chemistry Letters, 2020, 11, 1746-1752.	4.6	23
54	Cooperative Nitrogen Activation and Ammonia Synthesis on Densely Monodispersed Mo–N–C Sites. Journal of Physical Chemistry Letters, 2020, 11, 3962-3968.	4.6	23

#	Article	IF	CITATIONS
55	N-Doped Graphene-Supported Diatomic Ni–Fe Catalyst for Synergistic Oxidation of CO. Journal of Physical Chemistry C, 2021, 125, 5616-5622.	3.1	23
56	Zinc porphyrin-based electron donor–acceptor-conjugated microporous polymer for the efficient photocatalytic oxidative coupling of amines under visible light. Applied Catalysis A: General, 2020, 590, 117352.	4.3	21
57	Bandgap tuning of C3N monolayer: A first-principles study. Chemical Physics, 2019, 520, 40-46.	1.9	19
58	A machine learning vibrational spectroscopy protocol for spectrum prediction and spectrum-based structure recognition. Fundamental Research, 2021, 1, 488-494.	3.3	19
59	Suppressing Electron–Phonon Coupling through Laser-Induced Phase Transition. ACS Applied Materials & Interfaces, 2017, 9, 23309-23313.	8.0	18
60	Nickel nanograins anchored on a carbon framework for an efficient hydrogen evolution electrocatalyst and a flexible electrode. Journal of Materials Chemistry A, 2020, 8, 3499-3508.	10.3	18
61	Using Machine Learning to Predict the Dissociation Energy of Organic Carbonyls. Journal of Physical Chemistry A, 2020, 124, 3844-3850.	2.5	18
62	Role of Hydrogen Bonding in Green Fluorescent Protein-like Chromophore Emission. Scientific Reports, 2019, 9, 11640.	3.3	17
63	Emerging linear activity trend in the oxygen evolution reaction with dual-active-sites mechanism. Journal of Materials Chemistry A, 2020, 8, 20946-20952.	10.3	17
64	A stable triplet diradical emitter. Chemical Science, 2021, 12, 15151-15156.	7.4	17
65	Mechanistic Understanding towards the Role of Cyclohexene in Enhancing the Efficiency of Manganese Porphyrinâ€Catalyzed Aerobic Oxidation of Diphenylmethane. European Journal of Inorganic Chemistry, 2018, 2018, 2666-2674.	2.0	16
66	Kinetic Ionic Permeation and Interfacial Doping of Supported Graphene. Nano Letters, 2019, 19, 9029-9036.	9.1	16
67	Accurate Machine Learning Prediction of Protein Circular Dichroism Spectra with Embedded Density Descriptors. Jacs Au, 2021, 1, 2377-2384.	7.9	16
68	Machine learning recognition of protein secondary structures based on two-dimensional spectroscopic descriptors. Proceedings of the National Academy of Sciences of the United States of America, 2022, 119, e2202713119.	7.1	16
69	Promoting Intersystem Crossing of a Fluorescent Molecule via Single Functional Group Modification. Journal of Physical Chemistry Letters, 2019, 10, 1388-1393.	4.6	15
70	CO oxidation on Ru–Pt bimetallic nanoclusters supported on TiO2(101): The effect of charge polarization. Journal of Chemical Physics, 2018, 148, 124701.	3.0	14
71	A computational study on the tunability of woven covalent organic frameworks for photocatalysis. Physical Chemistry Chemical Physics, 2019, 21, 546-553.	2.8	14
72	Metal-enhanced hydrogenation of graphene with atomic pattern. Carbon, 2019, 143, 700-705.	10.3	14

#	Article	IF	CITATIONS
73	Identification of the protonation site of gaseous triglycine: the cis-peptide bond conformation as the global minimum. Physical Chemistry Chemical Physics, 2017, 19, 15030-15038.	2.8	13
74	Identifying the structure of 4-chlorophenyl isocyanide adsorbed on Au(111) and Pt(111) surfaces by first-principles simulations of Raman spectra. Physical Chemistry Chemical Physics, 2017, 19, 32389-32397.	2.8	12
75	Biomimetic Aerobic Epoxidation of Alkenes Catalyzed by Cobalt Porphyrin under Ambient Conditions in the Presence of Sunflower Seeds Oil as a Co-Substrate. ACS Omega, 2020, 5, 4890-4899.	3.5	12
76	Tuning Phase Transitions in Metal Oxides by Hydrogen Doping: A First-Principles Study. Journal of Physical Chemistry Letters, 2020, 11, 1075-1080.	4.6	12
77	Self-Adaptive Switch Enabling Complete Charge Separation in Molecular-Based Optoelectronic Conversion. Journal of Physical Chemistry Letters, 2018, 9, 837-843.	4.6	11
78	High-curvature carbon-supported Ni single atoms with charge polarization for highly efficient CO ₂ reduction. Chemical Communications, 2022, 58, 2914-2917.	4.1	11
79	Energy Materials Design for Steering Charge Kinetics. Advanced Materials, 2018, 30, e1801988.	21.0	10
80	Bimetallic Pd/Co Embedded in Two-Dimensional Carbon-Nitride for Z-Scheme Photocatalytic Water Splitting. Journal of Physical Chemistry C, 2019, 123, 1846-1851.	3.1	10
81	Photoswitchable de/adsorption of an azobenzene-derived surfactant on a silica surface. Physical Chemistry Chemical Physics, 2019, 21, 21030-21037.	2.8	9
82	Azopyrazole-Based Photoswitchable Anion Receptor for Dihydrogen Phosphate Transport. Journal of Physical Chemistry A, 2020, 124, 9692-9697.	2.5	9
83	Atomic Origin for Hydrogenation Promoted Bulk Oxygen Vacancies Removal in Vanadium Dioxide. Journal of Physical Chemistry Letters, 2020, 11, 10045-10051.	4.6	9
84	Sharp-tip enhanced catalytic CO oxidation by atomically dispersed Pt ₁ /Pt ₂ on a raised graphene oxide platform. Journal of Materials Chemistry A, 2020, 8, 12485-12494.	10.3	9
85	Enabling Efficient Charge Separation for Optoelectronic Conversion via an Energy-Dependent Z-Scheme n-Semiconductor–Metal–p-Semiconductor Schottky Heterojunction. Journal of Physical Chemistry Letters, 2020, 11, 3313-3319.	4.6	9
86	Identification of the smallest peptide with a zwitterion as the global minimum: a first-principles study on arginine-containing peptides. Physical Chemistry Chemical Physics, 2017, 19, 12117-12126.	2.8	8
87	"Healing―Effect of Graphene Oxide in Achieving Robust Dilute Ferromagnetism in Oxygen-Deficient Titanium Dioxide. Journal of Physical Chemistry C, 2017, 121, 22806-22814.	3.1	8
88	Fluorescent Molybdenum Oxide Quantum Dots and Hg ^{II} Synergistically Accelerate Cobalt Porphyrin Formation: A New Strategy for Trace Hg ^{II} Analysis. ACS Applied Nano Materials, 2018, 1, 1484-1491.	5.0	8
89	Zinc porphyrin and rhenium complex-based donor-acceptor conjugated porous polymer for visible-light-driven conversion of CO2 to CO. Journal of CO2 Utilization, 2022, 60, 101972.	6.8	8
90	Al-based spectroscopic monitoring of real-time interactions between SARS-CoV-2 and human ACE2. Proceedings of the National Academy of Sciences of the United States of America, 2021, 118, .	7.1	7

#	Article	IF	CITATIONS
91	A novel energy-dependent p-semiconductor–metal–n-semiconductor heterojunction for selectively steering charge flow in a <i>Z</i> -scheme photocatalyst. Journal of Materials Chemistry A, 2019, 7, 15036-15041.	10.3	6
92	Theoretical Calculation of Hydrogen Generation and Delivery via Photocatalytic Water Splitting in Boron–Carbon–Nitride Nanotube/Metal Cluster Hybrid. ACS Applied Materials & Interfaces, 2020, 12, 48684-48690.	8.0	6
93	Donor–Acceptor Type Conjugated Microporous Polymer as a Metal-Free Photocatalyst for Visible-Light-Driven Aerobic Oxidative Coupling of Amines. Catalysis Letters, 2021, 151, 3145-3153.	2.6	6
94	Imidazole-linked porphyrin-based conjugated microporous polymers for metal-free photocatalytic oxidative dehydrogenation of N-heterocycles. Sustainable Energy and Fuels, 2021, 5, 6478-6487.	4.9	6
95	Real-Time, Time-Dependent Density Functional Theory Study on Photoinduced Isomerizations of Azobenzene Under a Light Field. Journal of Physical Chemistry Letters, 2022, 13, 427-432.	4.6	6
96	Macroscopic Wires from Fluorophore-Quencher Dyads with Long-Lived Blue Emission. Journal of Physical Chemistry A, 2017, 121, 7183-7190.	2.5	5
97	Modulating Electron Transfer in an Organic Reaction via Chemical Group Modification of the Photocatalyst. Journal of Physical Chemistry Letters, 2019, 10, 5634-5639.	4.6	5
98	Tunable Single-Photon Emission by Defective Boron-Nitride Nanotubes for High-Precision Force Detection. Journal of Physical Chemistry C, 2019, 123, 9624-9628.	3.1	5
99	Regulation of Electronic Structure of Graphene Nanoribbon by Tuning Long-Range Dopant–Dopant Coupling at Distance of Tens of Nanometers. Journal of Physical Chemistry Letters, 2020, 11, 6907-6913.	4.6	5
100	Mechanism Study of Molecular Deformation of 2,2′,5′,2″-Tetramethylated <i>p</i> -Terphenyl-4,4″-dith Trapped in Gold Junctions. Journal of Physical Chemistry Letters, 2020, 11, 4456-4461.	io] 4.6	5
101	Edge-effect enhanced catalytic CO oxidation by atomically dispersed Pt on nitride-graphene. Journal of Materials Chemistry A, 2021, 9, 2093-2098.	10.3	5
102	Hydrogenated Oxide as Novel Quasi-metallic Cocatalyst for Efficient Visible-Light Driven Photocatalytic Water Splitting. Journal of Physical Chemistry C, 2021, 125, 12672-12681.	3.1	5
103	Synergistic effect of a diatomic boron-doped layered two-dimensional MSi ₂ N ₄ monolayer for an efficient electrochemical nitrogen reduction. Journal of Materials Chemistry A, 2022, 10, 14820-14827.	10.3	5
104	Probing flexible conformations in molecular junctions by inelastic electron tunneling spectroscopy. AIP Advances, 2015, 5, .	1.3	4
105	Structure-dependent luminescence of tetra-(4-pyridylphenyl)ethylene: a first-principles study. Physical Chemistry Chemical Physics, 2018, 20, 41-45.	2.8	4
106	Spatial Confinement of a Carbon Nanocone for an Efficient Oxygen Evolution Reaction. Journal of Physical Chemistry Letters, 2021, 12, 2252-2258.	4.6	4
107	Modulating Charge Separation and Intersystem Crossing in Donor–Switch–Acceptor Systems: A Computational Study. Journal of Physical Chemistry A, 2021, 125, 3088-3094.	2.5	4
108	Electron–Proton Coâ€dopingâ€Induced Metal–Insulator Transition in VO 2 Film via Surface Selfâ€Assembled l â€Ascorbic Acid Molecules. Angewandte Chemie, 2019, 131, 13849-13854.	2.0	3

#	Article	IF	CITATIONS
109	Theoretical Spectroscopic Studies on Chemical and Electronic Structures of Selenocysteine and Pyrrolysine. Journal of Physical Chemistry A, 2020, 124, 2215-2224.	2.5	3
110	Carbon Monoxide Oxidation Promoted by Surface Polarization Charges in a CuO/Ag Hybrid Catalyst. Scientific Reports, 2020, 10, 2552.	3.3	3
111	Bridged Azobenzene Enables Dynamic Control of Through-Space Charge Transfer for Photochemical Conversion. Journal of Physical Chemistry Letters, 2021, 12, 3868-3874.	4.6	3
112	Energy-Dependent Z-Scheme via Metal-Interfacing Two-Dimensional p-Type and n-Type Semiconductor Layers for Efficient Optoelectronic Conversion. Journal of Physical Chemistry Letters, 2019, 10, 4317-4322.	4.6	2
113	Competition between dispersion interactions and conventional hydrogen bonding: insights from a theoretical study on Z-Arg-OH. Physical Chemistry Chemical Physics, 2019, 21, 17893-17900.	2.8	2
114	Global Fold Switching of the RafH Protein: Diverse Structures with a Conserved Pathway. Journal of Physical Chemistry B, 2022, 126, 2979-2989.	2.6	2
115	Facile Removal of Bulk Oxygen Vacancy Defects in Metal Oxides Driven by Hydrogen-Dopant Evaporation. Journal of Physical Chemistry Letters, 2021, 12, 9579-9583.	4.6	1
116	Tuning Light Absorption in Platinum(II) Terpyridyl π-Conjugated Complexes: A First-Principle Study. Journal of Physical Chemistry A, 2017, 121, 5533-5539.	2.5	0